Strong Enhancement of Raman Scattering from a Bulk-Inactive Vibrational Mode in Few-Layer $MoTe_2$

Mahito Yamamoto,[†,#,*] Sheng Tsung Wang,[‡,#] Meiyan Ni,[†,§,#] Yen-Fu Lin,[†,⊥] Song-Lin Li,[†] Shinya Aikawa,[†] Wen-Bin Jian,[‡] Keiji Ueno,[∥] Katsunori Wakabayashi,[†] and Kazuhito Tsukagoshi[†,*]

[†]International Center for Materials Nanoarchitectonics (WPI-MANA), National Institute for Materials Science (NIMS), Tsukuba, Ibaraki 305-0044, Japan, [‡]Department of Electrophysics, National Chiao Tung University, Hsinchu 30010, Taiwan, [§]School of Electronic Science and Applied Physics, Hefei University of Technology, Hefei 230009, China, [⊥]Department of Physics, National Chung Hsing University, Taichung, 40227, Taiwan, and [∥]Department of Chemistry, Graduate School of Science and Engineering, Saitama University, Saitama 338-8570, Japan. [#]M. Yamamoto, S. T. Wang, and M. Ni contributed equally to this work.

ABSTRACT Two-dimensional layered crystals could show phonon properties that are markedly distinct from those of their bulk counterparts, because of the loss of periodicities along the *c*-axis directions. Here we investigate the phonon properties of bulk and atomically thin α-$MoTe_2$ using Raman spectroscopy. The Raman spectrum of α-$MoTe_2$ shows a prominent peak of the in-plane E^1_{2g} mode, with its frequency upshifting with decreasing thickness down to the atomic scale, similar to other dichalcogenides. Furthermore, we find large enhancement of the Raman scattering from the out-of-plane B^1_{2g} mode in the atomically thin layers. The B^1_{2g} mode is Raman inactive in the bulk, but is observed to become active in the few-layer films. The intensity ratio of the B^1_{2g} to E^1_{2g} peaks evolves significantly with decreasing thickness, in contrast with other dichalcogenides. Our observations point to strong effects of dimensionality on the phonon properties of $MoTe_2$.

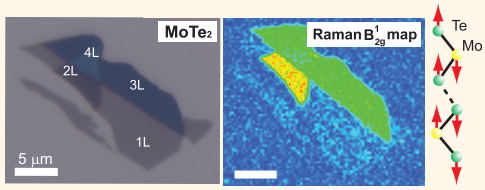

KEYWORDS: transition metal dichalcogenides · Raman spectroscopy · density functional theory · molybdenum ditelluride · MoS_2 · $MoSe_2$ · WSe_2

Atomic layers of group VI transition metal dichalcogenides (MX_2, where M = Mo and W and X = S, Se, and Te) have attracted much attention for a wide variety of applications ranging from spin- and valley-tronics to catalysts for hydrogen evolution reaction.[1−5] Of particular interest are their electronic and optoelectronic applications due to their large band gaps, together with the indirect-to-direct transitions in single-layers.[6−10] Field effect transistors with high on/off current ratios have been demonstrated using atomically thin MX_2.[11−14] Single-layers of MoS_2 and WSe_2 have been used in optoelectronic devices including photodetectors and photoemitters.[15−20] Thanks to their large mechanical strength,[21] few-layers of MoS_2 and WS_2 have been used to fabricate flexible electronic devices.[22−25] Additionally, atomically thin MX_2 films have potential for thermoelectric applications, owing to their low thermal conductivities.[26]

A crucial step toward the application of atomically thin MX_2 is to understand its phonon properties. Phonons couple to electrons and limit carrier mobility at room temperature,[27,28] along with Coulomb impurities.[29,30] Heat propagates in a crystal *via* predominantly acoustic phonons; thus, phonons determine its thermal conductivity.[31,32] Additionally, soft mode phonons determine the mechanical strength of the crystal.[33] Previously, Raman spectroscopy has been used to investigate the phonon properties of atomically thin MX_2, including electron−phonon coupling[34] and the effects of heating[35−37] and strain[38,39] on the phonons. Moreover, Raman spectroscopy has shown that the lattice dynamics in MoS_2, $MoSe_2$, WS_2, and WSe_2 depend sensitively on their thicknesses[40−43] and, hence, can be used to identify the number of layers at the atomic scale.

Here, we present, for the first time, Raman spectroscopy of atomically thin layers of α-$MoTe_2$. Bulk $MoTe_2$ is an indirect band gap semiconductor with a bandgap of 1.0 eV, but $MoTe_2$ is expected to exhibit a direct band gap of 1.1 eV in its single-layer,[44−46] similar to MoS_2, $MoSe_2$, WS_2, and WSe_2. Moreover, bulk $MoTe_2$ has been observed to undergo a transition from a diamagnetic

* Address correspondence to yamamoto.mahito@nims.go.jp, kazuhito.tsukagoshi@nims.go.jp.

Received for review February 7, 2014 and accepted March 21, 2014.

Published online March 21, 2014
10.1021/nn5007607

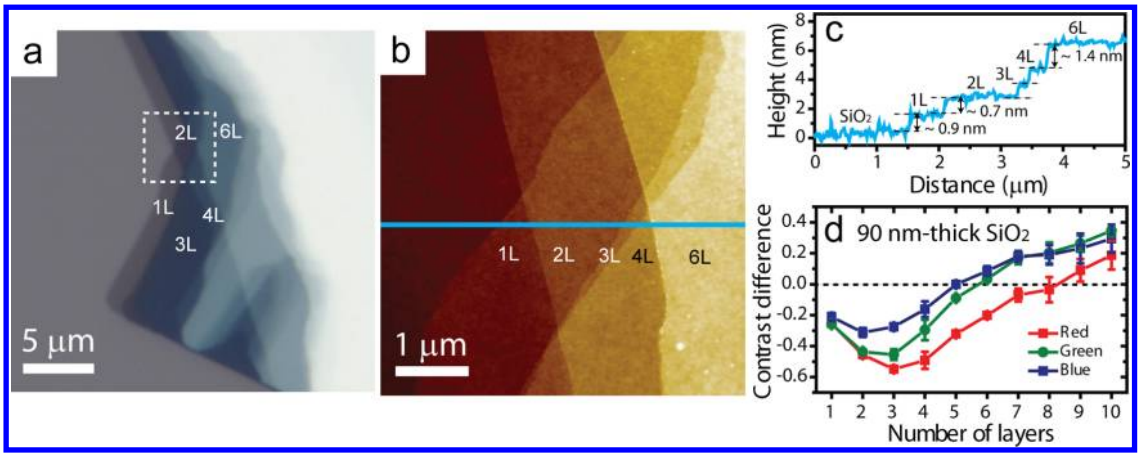

Figure 1. (a) Typical optical image of single- to multilayer $MoTe_2$ on 90 nm-thick SiO_2. The number of layers (*N*L with $N = 1-6$) is indicated. (b) An AFM image of the area surrounded by white dashed lines in (a). (c) A profile of the $MoTe_2$ flake along the blue line indicated in (b), showing a single-layer thickness of ~0.7 nm between the layers. (d) Optical contrast differences between the $MoTe_2$ and SiO_2 surfaces for the red, green, and blue channels of the optical images, as functions of thickness. The contrast difference is normalized with the optical contrast of SiO_2 for each channel.

semiconducting α-phase (trigonal prismatic) to a paramagnetic *β*-phase (distorted octahedral) at high temperatures,[47,48] offering unique potential for applications. However, though a few Raman spectroscopy studies of bulk $MoTe_2$ have been reported,[49−51] the lattice dynamics in atomically thin $MoTe_2$ has yet to be investigated.

The Raman spectrum of $MoTe_2$ shows a prominent peak of the in-plane E^1_{2g} mode at ~235 cm^{-1}, with a small out-of-plane A_{1g} peak at ~174 cm^{-1}. The E^1_{2g} mode upshifts, while the A_{1g} mode downshifts with decreasing thickness. Additionally, we find a strong peak at ~291 cm^{-1} in the atomically thin crystals. This peak is not observed in the bulk crystals, but the intensity is enhanced with decreasing thickness, down to bilayers. However, this peak is absent in single-layer $MoTe_2$. We assign, using density functional theory (DFT) and group theory analysis, the peak as a bulk-Raman inactive mode of B^1_{2g}. The activation of the B^1_{2g} mode in atomically thin $MoTe_2$ is due to translation symmetry breaking along the *c*-axis direction. These findings suggest strong effects of symmetry breaking on the phonon properties of atomically thin $MoTe_2$.

RESULTS AND DISCUSSION

Bulk crystals of $MoTe_2$ were prepared through chemical vapor transport,[52] and were determined to have a $2H_b$-structure (α-phase) by using X-ray photoelectron spectroscopy and X-ray diffraction.[14] Atomically thin $MoTe_2$ films were mechanically exfoliated from the bulk crystals onto silicon substrates with oxide layers on top. Figure 1a is a typical optical image of atomically thin $MoTe_2$ deposited on a 90 nm-thick SiO_2 substrate. We determine the thicknesses of the $MoTe_2$ films optically and using atomic force microscopy (AFM) in the tapping mode and Raman spectroscopy (see Figure S2 in Supporting Information for the identification of the number of layers from the Raman peak intensity ratios).[53] Figure 1b is an AFM image of the area inside the white dashed lines indicated in Figure 1a. The profile along the blue line in Figure 1b shows a single layer spacing of ~0.7 nm and a double layer spacing of ~1.4 nm (Figure 1c). Hence, the thickness of the flake in the scanned area is identified to be a single-layer- to six-layers-thick (Figure 1a,b). The larger height of single-layer $MoTe_2$ shown in Figure 1c is due to either trapped contaminations at the $MoTe_2-SiO_2$ interface, an artifact caused by the tapping mode AFM, or a combination of both.

We compare the optical contrasts between $MoTe_2$ of various thicknesses and the SiO_2 substrate to establish a reference for the identification of the number of layers. Figure 1d shows the optical contrast differences between the $MoTe_2$ and 90 nm-thick SiO_2 surfaces in gray scale for the red, green, and blue channels, as functions of the number of layers (the contrast difference is normalized with the contrast of the SiO_2 surface; see Methods and Section S3 in Supporting Information for details).[54] The contrast difference varies clearly with thickness up to 10 layers for each color channel and can be used to identify the thicknesses of the thin $MoTe_2$ films on SiO_2, similar to other two-dimensional dichalcogenides (see Figures S3 and S4 in Supporting Information for the optical and the corresponding gray scale images of $MoTe_2$ with various thicknesses and the optical contrast differences between the $MoTe_2$ and 285 nm-thick SiO_2 surfaces).[54−56]

The α-$MoTe_2$ crystal has a $2H_b-MX_2$ structure.[47,52] The $2H_b-MX_2$ crystal consists of layers of a trigonal prismatic X−M−X structure, as represented in Figure 2a. In the $2H_b$ structure, the X−M−X layers are stacked in an AbABaB sequence, where the upper and lower cases represent X and M atoms. Therefore, bulk $2H_b-MX_2$ belongs to the D^4_{6h} symmetry group with M and X atoms in the D_{3h} and C_{3v} point groups, respectively. The irreducible representations of the phonons in bulk MX_2

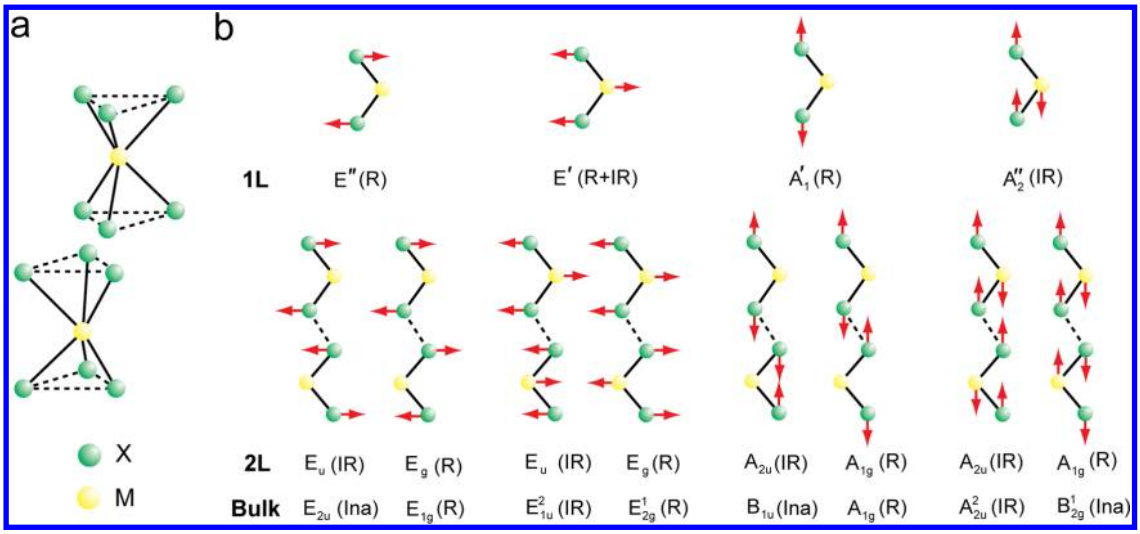

Figure 2. (a) Crystal structure of $2H_b-MX_2$ in a repeat unit (two layers). The metal (M) and chalcogen (X) atoms are represented in yellow and green, respectively. (b) Phonon modes of single-layer (1L), bilayer (2L), and bulk $2H_b-MX_2$ at the Γ point in the unit cell. Bilayer and bulk MX_2 have phonon modes with equivalent atomic displacements, but different irreducible representations and optical activities. "R", "IR", and "Ina" indicate the Raman active, infrared active, and optically inactive modes. The black dashed lines connecting the X atoms indicate interlayer interactions.

at the Brillion zone center (the Γ point) are

$$\Gamma_{bulk} = A_{1g} + 2A_{2u} + 2B_{2g} + E_{1g} + 2E_{1u} + E_{2u} + B_{1u} + 2E_{2g} \quad (1)$$

where E_{1g}, E^1_{2g}, E^2_{2g}, and A_{1g} are Raman-active and E^1_{1u}, E^2_{1u}, A^1_{2u}, and A^2_{2u} are infrared active. The other modes are optically inactive. (Figure 2b; see also Figure S1 in Supporting Information for atomic displacements of all the Γ point phonon modes in bulk $2H_b-MX_2$). Because of the loss of translation symmetry along the *c*-axis direction, single- and few-layers of $2H_b-MX_2$ belong to different space groups, depending on the parity of the number of layers. Atomically thin crystals with an odd number of layers belong to the D^1_{3h} symmetry group without inversion symmetry, while crystals with an even number of layers belong to the D^3_{3d} symmetry group with inversion symmetry.[57,58] The irreducible representations of the Γ point phonons of the *N*-layer MX_2 are thus

$$\Gamma_{odd} = \frac{3N-1}{2}(A_1' + E'') + \frac{3N+1}{2}(A_2'' + E') \quad (2a)$$

for an odd number of *N* and

$$\Gamma_{even} = \frac{3N}{2}(A_{1g} + A_{2u} + E_g + E_u) \quad (2b)$$

for an even number of *N*, respectively.[57,58] Group theory predicts that the phonon modes in the single- and few-layer crystals exhibit different optical activities from those of the corresponding modes in the bulk. Among the phonon modes in single- and few-layer MX_2, A_1', E'', A_{1g}, and E_g are Raman active, A_2'', A_{2u}, and E_u are infrared active, and E' is both Raman and infrared active. In Figure 2b, we find some phonon modes have equivalent atomic displacements but have different optical activities for single- and bilayer and bulk MX_2. For example, the bulk-inactive E_{2u} mode becomes infrared active for bilayers (E_u) and Raman active for a single-layer (E''). Below, we denote the phonon modes of atomically thin crystals with the irreducible representations of the corresponding modes in the bulk, according to the literature. Raman spectroscopy of atomically thin $2H_b-MoS_2$, $MoSe_2$, WS_2, and WSe_2 has shown peaks of the in-plane E^1_{2g} and out-of-plane A_{1g} modes.[40−43] Furthermore, peaks of an interlayer shear mode of E^2_{2g} have been observed at very low frequencies in few-layer MoS_2 and WSe_2.[57,59−61] The E_{1g} mode is forbidden in the backscattering configuration in the bulk, but has been detected in few-layers of WSe_2.[58]

We performed Raman spectroscopy of $MoTe_2$, using a solid-state laser with an excitation wavelength of 532 nm and a grating with 1800 grooves per millimeter, unless otherwise noted. Figure 3a shows the Raman spectra of single- to five- and 30-layer $MoTe_2$. The $MoTe_2$ films show prominent peaks of the E^1_{2g} mode at ∼235 cm^{-1} and relatively weak peaks of the A_{1g} mode at ∼174 cm^{-1}, as previously observed in the bulk crystals.[49−51] The frequencies of these modes in $MoTe_2$ are smaller than those observed in MoS_2 and $MoSe_2$ because of the larger weight of Te (see Section S4 in Supporting Information for the peak positions of the E^1_{2g} and A_{1g} modes in MoS_2, $MoSe_2$, and $MoTe_2$).[8,40] The peak near 235 cm^{-1} splits into two lines in 30-layer $MoTe_2$. While one of the peaks is the E^1_{2g} mode, another peak may be an infrared active mode of E^2_{1u} (the two modes are a conjugate pair with almost the same frequencies with a small shift induced by the interlayer interactions; see Figure 2b). The Raman activation of the E^2_{1u} mode has been reported in bulk MoS_2 under the resonance condition,[62,63] but the cause of the activation

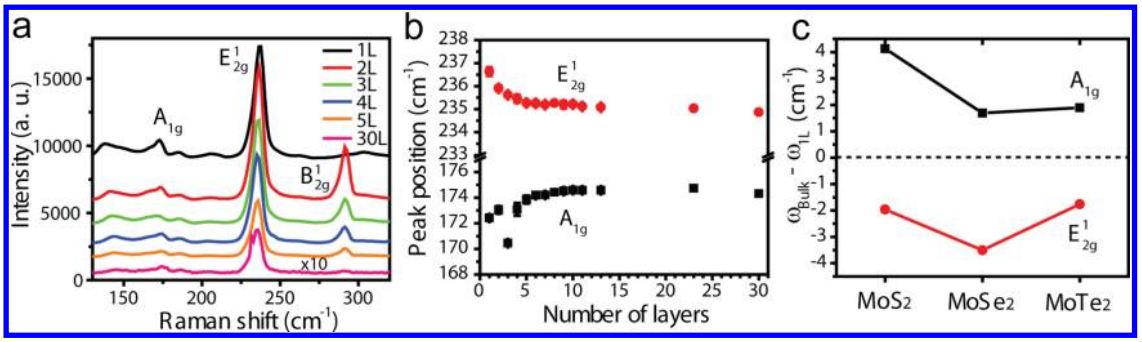

Figure 3. (a) Raman spectra of single- to five-layer and 30-layer $MoTe_2$. The excitation wavelength is 532 nm. The Raman intensity of 30-layer $MoTe_2$ is magnified by 10 times. The peak at ~291 cm^{-1} in few-layer $MoTe_2$ is identified as the B^1_{2g} mode in the text. (b) Peak positions of E^1_{2g} (red circles) and A_{1g} (black squares) for $MoTe_2$ as functions of the number of layers. (c) Frequency differences between the bulk and single-layer crystals, $\omega_{bulk} - \omega_{1L}$, for MoS_2, $MoSe_2$, and $MoTe_2$. The red circles represent the E^1_{2g} mode, and the black squares represent the A_{1g} mode.

in $MoTe_2$ is unclear. We observe small peaks near 138 and 185 cm^{-1}. These peaks may be the second-order Raman modes, as observed in other dichalcogenides.[41−43]

Figure 3b shows the peak positions of the E^1_{2g} and A_{1g} modes in $MoTe_2$ as functions of thickness. We find the E^1_{2g} mode upshifts by ~1.5 cm^{-1}, while the A_{1g} mode downshifts by ~2 cm^{-1}, with decreasing the number of layers from 30-layers to single-layer, as observed in other dichalcogenides.[40−43] The softening of the A_{1g} mode in atomically thin layers is caused by the smaller effects of interlayer interactions that induce restoring forces to $MoTe_2$ molecules,[40] while the stiffening of the E^1_{2g} mode may be due to effects of the boundary surface layers that lead to more effective forces to the $MoTe_2$ molecules with decreasing thickness.[64] We observe consistently an abrupt decrease in the A_{1g} frequency at trilayer thickness. The A_{1g} peak in trilayer $MoTe_2$ may be its "in-phase" vibrational mode, where the Te atoms in all three layers vibrate in phase (in the "out-of-phase" mode, the Te atoms in the middle layer vibrate 180° out-of-phase with respect to the outside layers). The "in-phase" and "out-of-phase" A_{1g} modes in trilayer $MoTe_2$ are expected to have lower and higher frequencies, respectively, than the A_{1g} mode of single-layer $MoTe_2$, because of interlayer interactions.[65] However, we observe no clear peak of the "out-of-phase" A_{1g} mode in trilayer $MoTe_2$, likely because of the low spectral resolution of our Raman measurements. Further work using higher resolution Raman spectroscopy is needed to determine the cause of a decrease in the A_{1g} frequency at trilayer thickness.

Figure 3c shows the frequency differences $\omega_{bulk} - \omega_{1L}$ for MoS_2, $MoSe_2$, and $MoTe_2$, where ω_{bulk} and ω_{1L} are the frequencies of the E^1_{2g} and A_{1g} modes of the bulk and single-layer crystals, respectively (see Section S4 in Supporting Information for the thickness-dependence of the E^1_{2g} and A_{1g} mode frequencies in MoS_2 and $MoSe_2$). For the A_{1g} mode, MoS_2 shows larger $\omega_{bulk} - \omega_{1L}$ than $MoSe_2$ and $MoTe_2$, while $MoSe_2$ and $MoTe_2$ show the small difference in $\omega_{bulk} - \omega_{1L}$. We also find no clear dependence of $\omega_{bulk} - \omega_{1L}$ on compounds for the E^1_{2g} mode. These observations imply that the frequency difference between the bulk and single-layer crystals has a complex variation for the compounds, depending on the interlayer interactions, the molecular weights, and the surface effects.[64]

In addition to the E^1_{2g} peak, we observe consistently a strong peak at ~291 cm^{-1} in atomically thin $MoTe_2$ (Figure 3a), which has been previously unassigned in Raman spectroscopy of bulk $MoTe_2$.[49−51] This peak is also observed using a 633 nm excitation wavelength (see Figure S8 in Supporting Information for the Raman spectrum). Figure 4a plots the intensity ratio of the peak at ~291 cm^{-1} to the E^1_{2g} peak as a function of thickness. The relative intensity is enhanced significantly with decreasing thickness and becomes the strongest in bilayer $MoTe_2$. However, the peak is invariably absent in single-layer $MoTe_2$, as shown in Figure 3a. The peak position has no clear thickness dependence (inset of Figure 4a). To investigate the spatial variation of the peak intensity, we perform Raman intensity mapping of atomically thin $MoTe_2$. Figure 4c is a Raman intensity map of the E^1_{2g} mode (~ 235 cm^{-1}) of the single- to few-layer flake shown in Figure 4b. The Raman map shows a homogeneous intensity distribution over the surfaces of each layer, except at the edges, indicating that the crystal quality is spatially uniform. Raman intensity mapping of the peak at ~291 cm^{-1} on the same flake in Figure 4d shows no detectable intensity in the single-layer regions, but strong intensities are observed in the bilayer region. The intensity is reduced on tri- and four-layer surfaces. Similar to the E^1_{2g} peak mapping, the peak intensity shows small spatial variations for each layer thickness.

These observations suggest that the phonon mode at ~291 cm^{-1} is Raman inactive in the bulk, but is intrinsically Raman-active in few-layer $MoTe_2$, rather than activated externally, *e.g.*, by defects or oxidation of $MoTe_2$.[62] To identify the phonon mode of the peak at 291 cm^{-1}, we calculate all of the phonon modes of α-$MoTe_2$ at the Γ point for single- to trilayer and bulk

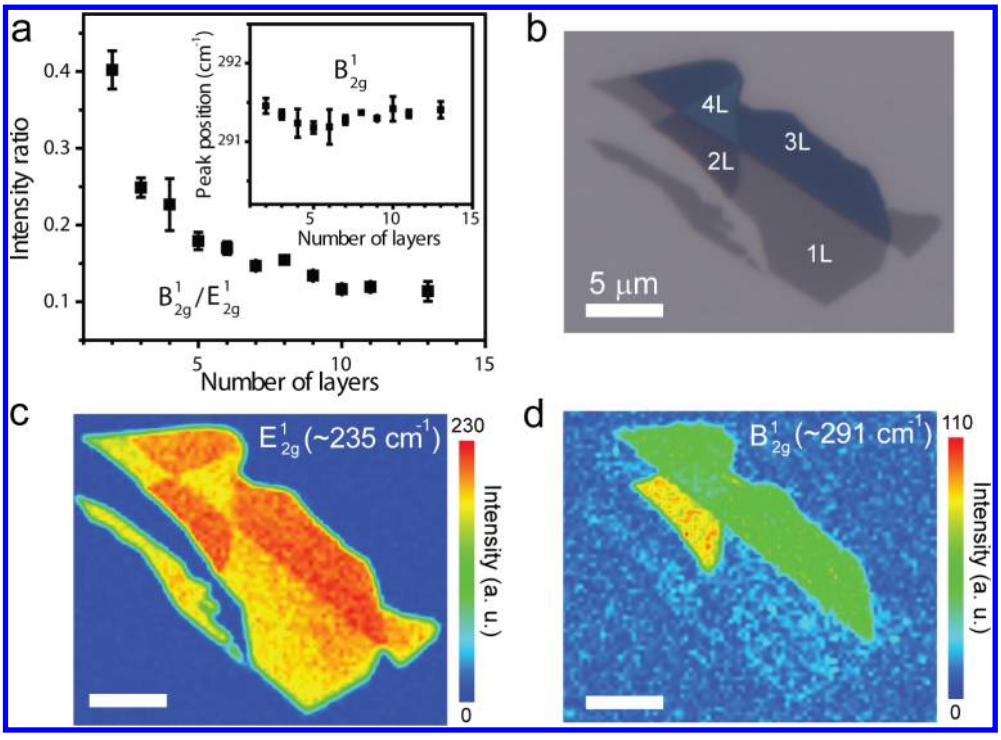

Figure 4. (a) Intensity ratio of the peak at ~291 cm^{-1} (which is identified to be the B^1_{2g} mode in the text) to the E^1_{2g} peak of $MoTe_2$, as a function of the number of layers. The inset is a plot of the peak position of the B^1_{2g} mode as a function of the number of layers. (b) An optical image of single- and few-layer $MoTe_2$ on 90 nm-thick SiO_2. The number of layers (*N*L with *N* = 1 to 4) is indicated. (b,c) Raman intensity maps of the $MoTe_2$ films shown in (b) at frequencies of (c) ~ 235 cm^{-1} and (d) ~ 291 cm^{-1}. The background intensities are subtracted. The scale bars are 5 μm.

TABLE 1. Calculated Frequencies (in cm^{-1}) of the Γ Point Phonon Modes of Single-Layer (1L), Bilayer (2L), Trilayer (3L), and Bulk Crystals of α-$MoTe_2$[a]

	in-plane				out-of-plane			
1L	E″ (R) 120.2		E′ (R+IR) 242.3		A_1' (R) 178.1		A_2'' (IR) 300.5	
2L	E_u (IR) 119.8	E_g (R) 121.0	E_u (IR) 241.0	E_g (R) 241.0	A_{2u} (IR) 177.9	A_{1g} (R) 180.2	A_{2u} (IR) 297.7	A_{1g} (R) 298.7
3L	E″(R) 121.4		E′ (R+IR) 241.0		A_1' (R) 179.4		A_1' (R) 298.5	
	E′ (R+IR) 120.5		E″ (R) 241.0		A_2'' (IR) 178.3		A_2'' (IR) 298.2	
	E″ (R) 119.7		E′ (R+IR) 239.9		A_1' (R) 177.0		A_2'' (IR) 295.9	
bulk	E_{2u} (Ina) 119.3	E_{1g} (R) 121.6	E^2_{1u} (IR) 239.8	E^1_{2g} (R) 239.9	B_{1u} (Ina) 176.3	A_{1g} (R) 179.9	A^2_{2u} (IR) 290.4	B^1_{2g} (Ina) 296.9

[a] Only high frequency phonons are shown. "R", "IR", and "Ina" indicate Raman- and infrared-active modes and optically inactive modes. The Raman/infrared activities of the phonon modes are determined from group theory.

crystals, by employing DFT. The DFT calculations were performed using the Vienna ab Simulation Package (VASP) within the local density approximation (LDA; see Methods for details).[66,67] Table 1 shows the calculated frequencies of the Γ-point phonon modes for single- to trilayer and bulk crystals of α-$MoTe_2$ with their Raman/infrared activities, determined by group theory (see Section S6 in Supporting Information for all the phonon frequencies calculated with DFT). The calculated frequencies of the E^1_{2g} and A_{1g} modes in bulk $MoTe_2$ and the corresponding modes in single- and few-layer $MoTe_2$ crystals are in reasonable agreement with the observed peak positions for each layer thickness, thus demonstrating the validity of the DFT calculations. In Table 1, we find no Raman-active modes near 291 cm^{-1} in single-layer and bulk $MoTe_2$, which is in consistent with the observations. The bi- and trilayer $MoTe_2$ crystals both have Raman-active modes of A_{1g} and A_1' near the observed peak positions of 291 cm^{-1}. Additionally, the Raman active A_{1g} mode is present near 291 cm^{-1} in four-layer $MoTe_2$ (see Table S2 in Supporting Information for the calculated frequencies of the phonon modes of four-layer $MoTe_2$). Thus, we conclusively assign the observed peaks in few-layer $MoTe_2$ at ~291 cm^{-1} as the out-of-plane vibrational modes of A_{1g} for an even number of layers and A_1' for an odd number of layers.

The A_{1g} and A_1' modes in few-layer crystals correspond to the B^1_{2g} mode in the bulk, which is optically inactive in $2H_b$–MX_2 (see Figure 2 and Table 1).

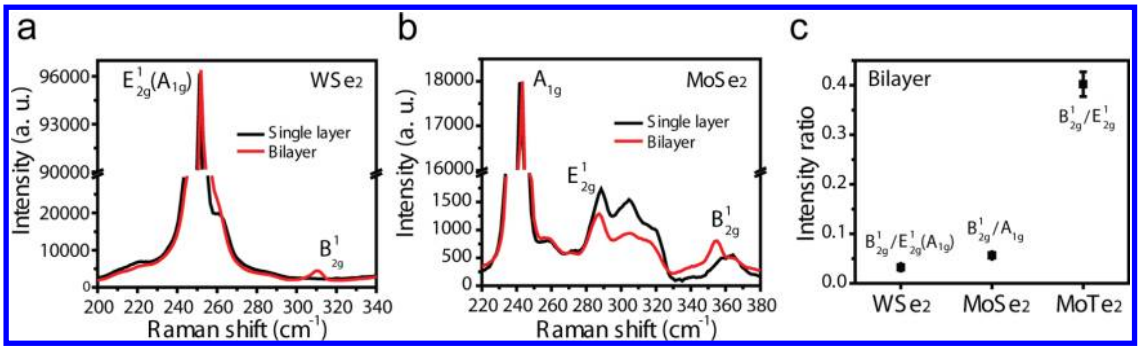

Figure 5. (a,b) Raman spectra of single-layer (black lines) and bilayers (red lines) of (a) WSe_2 and (b) $MoSe_2$. The E^1_{2g} peak intensities of the bilayer crystals are normalized with those of the single-layer crystals. (c) The intensity ratio of the B^1_{2g} peak to each prominent peak (either E^1_{2g} or A_{1g}) of bilayer WSe_2, $MoSe_2$, and $MoTe_2$.

A recent Raman spectroscopy study, along with DFT calculations and group theory analysis has reported that the B^1_{2g} mode of WSe_2 becomes Raman active at the two-dimensional limit, because of translation symmetry breaking.[58] Furthermore, few-layer $MoSe_2$ has been observed to show a weak Raman peak possibly from the B^1_{2g} mode.[65] Symmetry-breaking-induced Raman activation of a vibrational mode has also been observed in different groups of layered materials such as Bi_2Te_3 and Bi_2Se_3.[68−70] The peak intensities of the symmetry-breaking-activated modes are reduced with increasing the number of layers because the crystals become more bulk-like with thickness. Indeed, we find the intensity ratio of the B^1_{2g} peak to the E^1_{2g} peak in $MoTe_2$ decreases with increasing thickness (Figure 4a). Accordingly, we determine crystal symmetry breaking along the *c*-axis direction as the cause of the Raman activation of the B^1_{2g} mode in few-layer $MoTe_2$. However, the B^1_{2g} peak in atomically thin $MoTe_2$ is more strongly enhanced than in $MoSe_2$ and WSe_2. Figure 5a,b are Raman spectra of single- and bilayer WSe_2 and $MoSe_2$ flakes that are mechanically cleaved from the bulk crystals onto 285 nm-thick SiO_2. The WSe_2 and $MoSe_2$ bilayers show peaks of the B^1_{2g} mode at ~310 and ~355 cm^{-1}, which are absent in their single-layers. The intensities of the B^1_{2g} peaks in WSe_2 and $MoSe_2$ are extremely weak, compared with those of their most prominent peaks of the E^1_{2g} or A_{1g} modes (the E^1_{2g} and A_{1g} modes are nearly degenerate in WSe_2 and, thus, they are indistinguishable experimentally in our Raman measurements). In Figure 5c, we show the intensity ratio of the B^1_{2g} peak to each prominent peak of bilayer WSe_2, $MoSe_2$, and $MoTe_2$. The relative intensities of the B^1_{2g} peaks of WSe_2 and $MoSe_2$ are nearly 10 times smaller than that of $MoTe_2$. The strong enhancement of the B^1_{2g} peak intensity in atomically thin $MoTe_2$ is likely due to the large polarizability of the Te atom.[50] Additionally, the B^1_{2g} peak is persistently observed in $MoTe_2$ with thicknesses ranging from two- to 13-layers, as shown in Figure 4a, but is diminished rapidly within several-layers in WSe_2 and $MoSe_2$.[58,65] These results suggest strong effects of dimensionality on the Raman activity of the B^1_{2g} mode in $MoTe_2$.

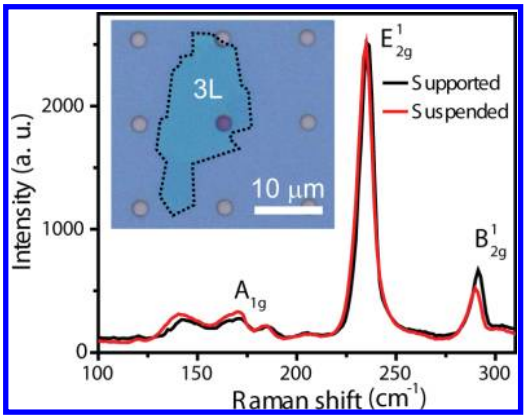

Figure 6. Raman spectra of trilayer (3L) $MoTe_2$ supported on SiO_2 (black line) and suspended over a hole (red line). The Raman spectrum of the suspended $MoTe_2$ flake is normalized with the E^1_{2g} peak intensity of the supported $MoTe_2$ flake. The inset is an optical image of 3L $MoTe_2$ on 300 nm-thick SiO_2 with periodic arrays of holes with diameters of 2 μm. The edge of the $MoTe_2$ flake is highlighted by the black dashed lines.

In addition to translation symmetry breaking, the optical activity of a vibrational mode in an atomically thin layered material might change due to coupling to an underlying substrate. Raman spectroscopy of atomically thin $2H_b$−$TaSe_2$ supported on SiO_2 shows a peak of the Raman E_{1g} mode that is forbidden in the backscattering geometry, but this peak is observed to be absent in free-standing $TaSe_2$. The observations imply that interactions between $TaSe_2$ and SiO_2 lead to the Raman-activation of the E_{1g} mode.[71] Lastly, we investigate the substrate effects on the Raman spectrum of atomically thin $MoTe_2$. The atomically thin $MoTe_2$ films were exfoliated onto SiO_2 substrates that were prepatterned with arrays of pits with diameters of 2−5 μm. The inset in Figure 6 is an optical image of trilayer $MoTe_2$ deposited on a SiO_2 substrate with pits with diameters of 2 μm. Figure 6 shows the Raman spectra of trilayer $MoTe_2$, supported on SiO_2 and suspended over a pit. Both the supported- and suspended-$MoTe_2$ films show the B^1_{2g} peaks with small differences in the

intensities, suggesting no obvious effect from the substrate on its Raman activation. Furthermore, we observe a small peak of the E_{1g} mode at ~120 cm^{-1} in both the supported- and suspended-$MoTe_2$ samples (see Figure S9 in Supporting Information for the expanded Raman spectra of $MoTe_2$ near ~120 cm^{-1}). Thus, in contrast with $TaSe_2$, the activation of the E_{1g} mode in trilayer $MoTe_2$ is due to crystal symmetry breaking rather than substrate effects, as previously observed in WSe_2.[58] We find the suspended $MoTe_2$ films show lower Raman frequencies than the supported-$MoTe_2$ films. The redshift in the Raman peaks in the suspended films is due to the larger thermal effects induced by the incident laser, because of the lack of heat dissipation paths.[35−37]

CONCLUSIONS

In summary, we have exfoliated atomically thin crystals of α-$MoTe_2$ and investigated their thickness-dependent phonon properties with Raman spectroscopy. Similar to other dichalcogenides, the Raman E^1_{2g} peak of $MoTe_2$ upshifts, while the A_{1g} peak downshifts, with decreasing thickness down to the atomic scale. However, we have observed a strong peak in atomically thin $MoTe_2$, which has been unassigned in bulk $MoTe_2$. The peak intensity is enhanced largely with decreasing thickness, but the peak vanishes at single-layer thickness. We assign, by using group theory and DFT calculations within LDA, the observed peak as the bulk-Raman inactive B^1_{2g} mode. The activation of the B^1_{2g} peak at atomically thin thickness is due to translation symmetry breaking along the *c*-axis direction, rather than substrate effects. The relative peak intensity of the B^1_{2g} mode in atomically thin $MoTe_2$ is much stronger than those observed in WSe_2 and $MoSe_2$. These observations suggest strong effects of symmetry breaking on the phonon properties of atomically thin $MoTe_2$. In contrast to other dichalcogenides, very little is known about the electronic and optical properties of $MoTe_2$ in its atomically thin form. Our results could provide insight into the phonon properties of atomically thin $MoTe_2$ and also a strategy for identifying the number of layers of $MoTe_2$ at the atomic scale for further studies.

METHODS

Experimental Details. Bulk crystals of α-$MoTe_2$, $2H_b$−$MoSe_2$, and $2H_b$−WSe_2 were synthesized through chemical vapor transport.[52] For MoS_2, commercially available crystals were used (Furuuchi Chemical Corporation). Atomically thin crystals of $MoTe_2$, MoS_2, $MoSe_2$, and WSe_2 were exfoliated mechanically from the bulk crystals onto SiO_2 with a thickness of either 90 or 285 nm, using adhesive tape. To obtain the suspended $MoTe_2$ samples, atomically thin $MoTe_2$ films were deposited onto 300 nm-thick SiO_2 substrates that were prepatterned with periodic arrays of pits with diameters ranging from 2 to 5 μm. The patterns were fabricated using photolithography and dry etching processes. The thicknesses of the atomically thin crystals were identified optically and with Raman spectroscopy and atomic force microscopy.[40,43,53] For the optical contrast analysis, gray scale images were extracted from the bare optical images for the red, green, and blue components by using ImageJ.[54] Raman spectroscopy was performed in the backscattering configuration using 532 and 633 nm excitation lasers, a 100× objective, and a grating with 1800 grooves/mm (Tokyo Instruments, Inc.). The laser power was kept below 0.1 mW to avoid any damage to the samples. Atomic force microscopy was performed at room temperature in the tapping mode with silicon cantilevers (Seiko Instruments Inc.).

Calculation Details. Density functional theory calculations were performed using the Vienna ab Simulation Package.[66,67] The core and valence electrons in the atoms were described with the projector-augmented wave method. The exchange-correlation functional was treated with the local density approximation, which gives a good description of the geometrical and phonon properties of layered materials. The plane-wave basis set cutoff was 500 eV for $MoTe_2$. Monkhorst-Pack k-point meshes of 9 × 9 × 1 and 9 × 9 × 5 were used for the thin films and the bulk, respectively. To avoid interactions between the periodic images of the thin films in the stacking direction, a vacuum thickness of 15 Å was used. All of the structures were completely optimized with convergence thresholds of 10^{-6} eV for the energies and 10^{-3} eV/Å for the forces. The phonon frequencies and eigenvectors were calculated using density functional perturbation theory.

Conflict of Interest: The authors declare no competing financial interest.

Acknowledgment. We thank Yasushi Morihira and Hiroyuki Watabe from Tokyo Instruments, Inc., for their technical support in the Raman measurement. This research was supported by a Grant-in-Aid (Kakenhi No. 25107004) from the Japan Society for the Promotion of Science (JSPS) through the Funding Program for World-Leading Innovative R&D on Science and Technology (FIRST), initiated by the Council for Science and Technology Policy (CSTP) of Japan, and Experiment-Theory Fusion trial project by MANA.

Supporting Information Available: The Γ-point phonon modes of bulk $2H_b$−MX_2, identification of the number of layers of $MoTe_2$ from the Raman intensity ratios, optical contrast differences between atomically thin $MoTe_2$ and SiO_2 surfaces, peak positions and intensities of the E^1_{2g} and A_{1g} modes and their thickness-dependences for MoS_2, $MoSe_2$, and $MoTe_2$, the 633 nm-excited Raman spectrum of atomically thin $MoTe_2$, the calculated phonon frequencies of $MoTe_2$, and Raman spectra of supported- and suspended-$MoTe_2$. This material is available free of charge *via* the Internet at http://pubs.acs.org.

REFERENCES AND NOTES

1. Wang, Q. H.; Kalantar-Zadeh, K.; Kis, A.; Coleman, J. N.; Strano, M. S. Electronics and Optoelectronics of Two-Dimensional Transition Metal Dichalcogenides. *Nat. Nanotechnol.* **2012**, *7*, 699–712.
2. Chhowalla, M.; Shin, H. S.; Eda, G.; Li, L. -J.; Loh, K. P.; Zhang, H. The Chemistry of Two-Dimensional Layered Transition Metal Dichalcogenide Nanosheets. *Nat. Chem.* **2013**, *5*, 263–275.
3. Butler, S. Z.; Hollen, S. M.; Cao, L.; Cui, Y.; Gupta, J. A.; Gutiérrez, H. R.; Heinz, T. F.; Hong, S. S.; Huang, J.; Ismach, A. F.; *et al.* Progress, Challenges, and Opportunities in Two-Dimensional Materials Beyond Graphene. *ACS Nano* **2013**, *7*, 2898–2926.
4. Xu, M.; Liang, T.; Shi, M.; Chen, H. Graphene-like Two-Dimensional Materials. *Chem. Rev.* **2013**, *113*, 3766–3798.
5. Song, X.; Hu, J.; Zeng, H. Two-Dimensional Semiconductors: Recent Progress and Future Perspectives. *J. Mater. Chem. C* **2013**, *1*, 2952–2969.
6. Mak, K. F.; Lee, C.; Hone, J.; Shan, J.; Heinz, T. F. Atomically Thin MoS_2: A New Direct-Gap Semiconductor. *Phys. Rev. Lett.* **2010**, *105*, 136805.
7. Splendiani, A.; Sun, L.; Zhang, Y.; Li, T.; Kim, J.; Chim, C. -Y.; Galli, G.; Wang, F. Emerging Photoluminescence in Monolayer MoS_2. *Nano Lett.* **2010**, *10*, 1271–1275.

8. Tongay, S.; Zhou, J.; Ataca, C.; Lo, K.; Matthews, T. S.; Li, J.; Grossman, J. C.; Wu, J. Thermally Driven Crossover from Indirect Toward Direct Bandgap in 2D Semiconductors: $MoSe_2$ *versus* MoS_2. *Nano Lett.* **2012**, *12*, 5576–5580.
9. Gutiérrez, H. R.; Perea-López, N.; Elías, A. L.; Berkdemir, A.; Wang, B.; Lv, R.; López-Urías, F.; Crespi, V. H.; Terrones, H.; Terrones, M. Extraordinary Room-Temperature Photoluminescence in Triangular WS_2 Monolayers. *Nano Lett.* **2013**, *13*, 3447–3454.
10. Zhao, W.; Ghorannevis, Z.; Chu, L.; Toh, M.; Kloc, C.; Tan, P. -H.; Eda, G. Evolution of Electronic Structure in Atomically Thin Sheets of WS_2 and WSe_2. *ACS Nano* **2013**, *7*, 791–797.
11. Radisavljevic, B.; Radenovic, A.; Brivio, J.; Giacometti, V.; Kis, A. Single-Layer MoS_2 Transistors. *Nat. Nanotechnol.* **2011**, *6*, 147–150.
12. Fang, H.; Chuang, S.; Chang, T. C.; Takei, K.; Takahashi, T.; Javey, A. High-Performance Single Layered WSe_2 p-FETs with Chemically Doped Contacts. *Nano Lett.* **2012**, *12*, 3788–3792.
13. Larentis, S.; Fallahazad, B.; Tutuc, E. Field-Effect Transistors and Intrinsic Mobility in Ultra-Thin $MoSe_2$ Layers. *Appl. Phys. Lett.* **2012**, *101*, 223104.
14. Lin, Y. -F.; Xu, Y.; Wang, S. -T.; Li, S. -L.; Yamamoto, M.; Aparecido-Ferreira, A.; Li, W.; Sun, H.; Nakaharai, S.; Jian, W.-B.; *et al.* Ambipolar $MoTe_2$ Transistors and Their Applications in Logic Circuits. *Adv. Mater.*, accepted.
15. Yin, Z.; Li, H.; Li, H.; Jiang, L.; Shi, Y.; Sun, Y.; Lu, G.; Zhang, Q.; Chen, X.; Zhang, H. Single-Layer MoS_2 Phototransistors. *ACS Nano* **2012**, *6*, 74–80.
16. Lopez-Sanchez, O.; Lembke, D.; Kayci, M.; Radenovic, A.; Kis, A. Ultrasensitive Photodetectors Based on Monolayer MoS_2. *Nat. Nanotechnol.* **2013**, *8*, 497–501.
17. Sundaram, R. S.; Engel, M.; Lombardo, A.; Krupke, R.; Ferrari, A. C.; Avouris, P.; Steiner, M. Electroluminescence in Single Layer MoS_2. *Nano Lett.* **2013**, *13*, 1416–1421.
18. Baugher, B. W. H.; Churchill, H. O. H.; Yang, Y.; Jarillo-Herrero, P. Optoelectronic Devices Based on Electrically Tunable p−n Diodes in a Monolayer Dichalcogenide. *Nat. Nanotechnol.* **2014**, 10.1038/nnano.2014.25.
19. Ross, J. S.; Klement, P.; Jones, A. M.; Ghimire, N. J.; Yan, J.; Mandrus, D. G.; Taniguchi, T.; Watanabe, K.; Kitamura, K.; Yao, W.; *et al.* Electrically Tunable Excitonic Light-Emitting Diodes Based on Monolayer WSe_2 p−n Junctions. *Nat. Nanotechnol.* **2014**, 10.1038/nnano.2014.26.
20. Pospischil, A.; Furchi, M. M.; Mueller, T. Solar-Energy Conversion and Light Emission in an Atomic Monolayer p−n Diode. *Nat. Nanotechnol.* **2014**, 10.1038/nnano.2014.14.
21. Bertolazzi, S.; Brivio, J.; Kis, A. Stretching and Breaking of Ultrathin MoS_2. *ACS Nano* **2011**, *12*, 9703–9709.
22. Pu, J.; Yomogida, Y.; Liu, K. -K.; Li, L. -J.; Iwasa, Y.; Takenobu, T. Highly Flexible MoS_2 Thin-Film Transistors with Ion Gel Dielectrics. *Nano Lett.* **2012**, *12*, 4013–4017.
23. Salvatore, G. A.; Münzenrieder, N.; Barraud, C.; Petti, L.; Zysset, C.; Büthe, L.; Ensslin, K.; Tröster, G. Fabrication and Transfer of Flexible Few-Layers MoS_2 Thin Film Transistors to Any Arbitrary Substrate. *ACS Nano* **2013**, *7*, 8809–8815.
24. Lee, G. -H.; Yu, Y. -J.; Cui, X.; Petrone, N.; Lee, C. -H.; Choi, M. S.; Lee, D. -Y.; Lee, C.; Yoo, W. J.; Watanabe, K.; *et al.* Flexible and Transparent MoS_2 Field-Effect Transistors on Hexagonal Boron Nitride-Graphene Heterostrucures. *ACS Nano* **2013**, *7*, 7931–7936.
25. Yu, W. J.; Li, Z.; Zhou, H.; Chen, Y.; Wang, Y.; Huang, Y.; Duan, X. Vertically Stacked Multi-Heterostructures of Layered Materials for Logic Transistors and Complementary Inverters. *Nat. Mater.* **2013**, *12*, 246–252.
26. Huang, W.; Da, H.; Liang, G. Thermoelectric Performance of MX_2 (M = Mo, W; X= S, Se) Monolayers. *J. Appl. Phys.* **2013**, *113*, 104304.
27. Kaasbjerg, K.; Thygesen, K. S.; Jacobsen, K. W. Phonon-Limited Mobility in *n*-Type Single-Layer MoS_2 from First Principles. *Phys. Rev. B: Condens. Matter Mater. Phys.* **2012**, *85*, 115317.
28. Kaasbjerg, K.; Thygesen, K. S.; Jauho, A. -P. Acoustic Phonon Limited Mobility in Two-Dimensional Semiconductors: Deformation Potential and Piezoelectric Scattering in Monolayer MoS_2 from First Principles. *Phys. Rev. B: Condens. Matter Mater. Phys.* **2013**, *87*, 235312.
29. Ghatak, S.; Pal, A. N.; Ghosh, A. Nature of Electronic States in Atomically Thin MoS_2 Field-Effect Transistors. *ACS Nano* **2011**, *5*, 7707–7712.
30. Li, S. -L.; Wakabayashi, K.; Xu, Y.; Nakaharai, S.; Komatsu, K.; Li, W. -W.; Lin, Y. -F.; Aparecido-Ferreira, A.; Tsukagoshi, K. Thickness-Dependent Interfacial Coulomb Scattering in Atomically Thin Field-Effect Transistors. *Nano Lett.* **2013**, *13*, 3546–3552.
31. Liu, X.; Zhang, G.; Pei, Q. -X.; Zhang, Y. -W. Phonon Thermal Conductivity of Monolayer MoS_2 Sheet and Nanoribbons. *Appl. Phys. Lett.* **2013**, *103*, 133113.
32. Li, W.; Carrete, J.; Mingo, N. Thermal Conductivity and Phonon Linewidths of Monolayer MoS_2 from First Principles. *Appl. Phys. Lett.* **2013**, *103*, 253103.
33. Li, T. Ideal Strength and Phonon Instability in Single-Layer MoS_2. *Phys. Rev. B: Condens. Matter Mater. Phys.* **2012**, *85*, 235407.
34. Chakraborty, B.; Bera, A.; Muthu, D. V. S.; Bhowmick, S.; Waghmare, U. V.; Sood, A. K. Symmetry-Dependent Phonon Renormalization in Monolayer MoS_2 Transistor. *Phys. Rev. B: Condens. Matter Mater. Phys.* **2012**, *85*, 161403(R).
35. Najmaei, S.; Liu, Z.; Ajayan, P. M.; Lou, J. Thermal Effects on the Characteristic Raman Spectrum of Molybdenum Disulfide (MoS_2) of Varying Thicknesses. *Appl. Phys. Lett.* **2012**, *100*, 013106.
36. Sahoo, S.; Gaur, A. P. S.; Ahmadi, M.; Guinel, M. J. -F.; Katiyar, R. S. Temperature-Dependent Raman Studies and Thermal Conductivity of Few-Layer MoS_2. *J. Phys. Chem. C* **2013**, *117*, 9042–9047.
37. Yan, R.; Simpson, J. R.; Bertolazzi, S.; Brivio, J.; Watson, M.; Wu, X.; Kis, A.; Luo, T.; Walker, A. R. H.; Xing, H. G. Thermal Conductivity of Monolayer Molybdenum Disulfide Obtained from Temperature-Dependent Raman Spectroscopy. *ACS Nano* **2014**, *8*, 986–993.
38. Rice, C.; Young, R. J.; Zan, R.; Bangert, U.; Wolverson, D.; Georgiou, T.; Jalil, R.; Novoselov, K. S. Raman-Scattering Measurements and First-Principles Calculations of Strain-Induced Phonon Shifts in Monolayer MoS_2. *Phys. Rev. B: Condens. Matter Mater. Phys.* **2013**, *87*, 081307(R).
39. Wang, Y.; Cong, C.; Qiu, C.; Yu, T. Raman Spectroscopy Study of Lattice Vibration and Crystallographic Orientation of Monolayer MoS_2 under Uniaxial Strain. *Small* **2013**, *9*, 2857–2861.
40. Lee, C.; Yan, H.; Brus, L. E.; Heinz, T. F.; Hone, J.; Ryu, S. Anomalous Lattice Vibrations of Single-and Few-Layer MoS_2. *ACS Nano* **2010**, *4*, 2695–2700.
41. Li, H.; Zhang, Q.; Yap, C. C. R.; Tay, B. K.; Edwin, T. H. T.; Olivier, A.; Baillargeat, D. From Bulk to Monolayer MoS_2: Evolution of Raman Scattering. *Adv. Funct. Mater.* **2012**, *22*, 1385–1390.
42. Berkdemir, A.; Gutiérrez, H. R.; Botello-Méndez, A. R.; Perea-López, N.; Elías, A. L.; Chia, C. -I.; Wang, B.; Crespi, V. H.; López-Urías, F.; Charlier, J. -C.; *et al.* Identification of Individual and Few Layers of WS_2 Using Raman Spectroscopy. *Sci. Rep.* **2013**, *3*, 1755.
43. Zhao, W.; Ghorannevis, Z.; Amara, K. K.; Pang, J. R.; Toh, M.; Zhang, X.; Kloc, C.; Tan, P. H.; Eda, G. Lattice Dynamics in Mono-and Few-Layer Sheets of WS_2 and WSe_2. *Nanoscale* **2013**, *5*, 9677–9683.
44. Ding, Y.; Wang, Y.; Ni, J.; Shi, L.; Shi, S.; Tang, W. First Principles Study of Structural, Vibrational and Electronic Properties of Graphene-like MX_2 (M = Mo, Nb, W, Ta; X = S, Se, Te) Monolayers. *Physica B* **2011**, *406*, 2254–2260.
45. Ataca, C.; Şahin, H.; Ciraci, S. Stable, Single-Layer MX2 Transition-Metal Oxides and Dichalcogenides in a Honeycomb-like Structure. *J. Phys. Chem. C* **2012**, *116*, 8983–8999.
46. Ma, Y.; Dai, Y.; Guo, M.; Niu, C.; Lu, J.; Huang, B. Electronic and Magnetic Properties of Perfect, Vacancy-Doped, and Nonmetal Adsorbed $MoSe_2$, $MoTe_2$ and WS_2 Monolayers. *Phys. Chem. Chem. Phys.* **2011**, *13*, 15546–15553.
47. Vellinga, M. B.; de Jonge, R.; Haas, C. Semiconductor to Metal Transition in $MoTe_2$. *J. Solid State Chem.* **1970**, *2*, 299–302.
48. Dawson, W. G.; Bullett, D. W. Electronic Structure and Crystallography of $MoTe_2$ and WTe_2. *J. Phys. C: Solid State Phys.* **1987**, *20*, 6159–6174.

49. Wieting, T. J.; Grisel, A.; Lévy, F. Interlayer Bonding and Localized Charge in $MoSe_2$ and α-$MoTe_2$. *Physica B* **1980**, *99*, 337–342.
50. Sugai, S.; Ueda, T. High-Pressure Raman Spectroscopy in the Layered Materials 2H-MoS_2, 2H-$MoSe_2$, and 2H-$MoTe_2$. *Phys. Rev. B: Condens. Matter Mater. Phys.* **1982**, *26*, 6554–6558.
51. Agnihotri, O. P.; Sehgal, H. K.; Garg, A. K. Laser Excited Raman Spectra of Gr. VI Semiconducting Compounds. *Solid State Commun.* **1973**, *12*, 135–138.
52. Lieth, R. M. A. *Preparation and Crystal Growth of Materials with Layered Structures*; Springer: Berlin, 1977; Vol. 1.
53. Li, S. -L.; Miyazaki, H.; Song, H.; Kuramochi, H.; Nakaharai, S.; Tsukagoshi, K. Quantitative Raman Spectrum and Reliable Thickness Identification for Atomic Layers on Insulating Substrates. *ACS Nano* **2012**, *6*, 7381–7388.
54. Li, H.; Wu, J.; Huang, X.; Lu, G.; Yang, J.; Lu, X.; Xiong, Q.; Zhang, H. Rapid and Reliable Thickness Identification of Two-Dimensional Nanosheets Using Optical Microscopy. *ACS Nano* **2013**, *7*, 10344–10353.
55. Castellanos-Gomez, A.; Agraït, N.; Rubio-Bollinger, G. Optical Identification of Atomically Thin Dichalcogenide Crystals. *Appl. Phys. Lett.* **2010**, *96*, 213116.
56. Castellanos-Gomez, A.; Navarro-Moratalla, E.; Mokry, G.; Quereda, J.; Pinilla-Cienfuegos, E.; Agraït, N.; van der Zant, H. S. J.; Coronado, E.; Steele, G. A.; Rubio-Bollinger, G. Fast and Reliable Identification of Atomically Thin Layers of $TaSe_2$ Crystals. *Nano Res.* **2013**, *6*, 191–199.
57. Zhao, Y.; Luo, X.; Li, H.; Zhang, J.; Araujo, P. T.; Gan, C. K.; Wu, J.; Zhang, H.; Quek, S. Y.; Dresselhaus, M. S.; *et al.* Interlayer Breathing and Shear Modes in Few-Trilayer MoS_2 and WSe_2. *Nano Lett.* **2013**, *13*, 1007–1015.
58. Luo, X.; Zhao, Y.; Zhang, J.; Toh, M.; Kloc, C.; Xiong, Q.; Quek, S. Y. Effects of Lower Symmetry and Dimensionality on Raman Spectra in Two-Dimensional WSe_2. *Phys. Rev. B: Condens. Matter Mater. Phys.* **2013**, *88*, 195313.
59. Plechinger, G.; Heydrich, S.; Eroms, J.; Weiss, D.; Schüller, C.; Korn, T. Raman Spectroscopy of the Interlayer Shear Mode in Few-Layer MoS_2 Flakes. *Appl. Phys. Lett.* **2012**, *101*, 101906.
60. Zeng, H.; Zhu, B.; Liu, K.; Fan, J.; Cui, X.; Zhang, Q. M. Low-Frequency Raman Modes and Electronic Excitations in Atomically Thin MoS_2 Films. *Phys. Rev. B: Condens. Matter Mater. Phys.* **2012**, *86*, 241301(R).
61. Zhang, X.; Han, W. P.; Wu, J. B.; Milana, S.; Lu, Y.; Li, Q. Q.; Ferrari, A. C.; Tan, P. H. Raman Spectroscopy of Shear and Layer Breathing Modes in Multilayer MoS_2. *Phys. Rev. B: Condens. Matter Mater. Phys.* **2013**, *87*, 115413.
62. Windom, B. C.; Sawyer, W. G.; Hahn, D. W. A Raman Spectroscopic Study of MoS_2 and MoO_3: Applications to Tribological Systems. *Tribol. Lett.* **2011**, *42*, 301–310.
63. Sekine, T.; Uchinokura, K.; Nakashizu, T.; Matsuura, E.; Yoshizaki, R. Dispersive Raman Mode of Layered Compound 2H-MoS_2 under Resonant Condition. *J. Phys. Soc. Jpn.* **1984**, *53*, 811–818.
64. Luo, X.; Zhao, Y.; Zhang, J.; Xiong, Q.; Quek, S. Y. Anomalous Frequency Trends in MoS_2 Thin Films Attributed to Surface Effects. *Phys. Rev. B: Condens. Matter Mater. Phys.* **2013**, *88*, 075320.
65. Tonndorf, P.; Schmidt, R.; Böttger, P.; Zhang, X.; Börner, J.; Liebig, A.; Albrecht, M.; Kloc, C.; Gordan, O.; Zahn, D. R. T.; *et al.* Photoluminescence Emission and Raman Response of Monolayer MoS_2, $MoSe_2$, and WSe_2. *Opt. Express* **2013**, *21*, 4908–4916.
66. Kresse, G.; Furthmüller, J. Efficiency of *Ab-Initio* Total Energy Calculations for Metals and Semiconductors Using a Plane-Wave Basis Set. *Comput. Mater. Sci.* **1996**, *6*, 15–50.
67. Kresse, G.; Furthmüller, J. Efficient Iterative Schemes for *Ab Initio* Total-Energy Calculations Using a Plane-Wave Basis Set. *Phys. Rev. B: Condens. Matter Mater. Phys.* **1996**, *54*, 11169–11186.
68. Shahil, K. M. F.; Hossain, M. Z.; Teweldebrhan, D.; Balandin, A. A. Crystal Symmetry Breaking in Few-Quintuple Bi_2Te_3 Films: Applications in Nanometrology of Topological Insulators. *Appl. Phys. Lett.* **2010**, *96*, 153103.
69. Teweldebrhan, D.; Goyal, V.; Balandin, A. A. Exfoliation and Characterization of Bismuth Telluride Atomic Quintuples and Quasi-Two-Dimensional Crystals. *Nano Lett.* **2010**, *10*, 1209–1218.
70. Shahil, K. M. F.; Hossain, M. Z.; Goyal, V.; Balandin, A. A. Micro-Raman Spectroscopy of Mechanically Exfoliated Few-Quintuple Layers of Bi_2Te_3, Bi_2Se_3, and Sb_2Te_3 Materials. *J. Appl. Phys.* **2012**, *111*, 054305.
71. Hajiyev, P.; Cong, C.; Qiu, C.; Yu, T. Contrast and Raman Spectroscopy Study of Single-and Few-Layered Charge Density Wave Material: 2H-$TaSe_2$. *Sci. Rep.* **2013**, *3*, 2593.